Hindawi Publishing Corporation
Journal of Nanotechnology
Volume 2011, Article ID 617196, 9 pages
doi:10.1155/2011/617196

Research Article

Intermediate Frequency AC Signal Analysis for Bionanosensor

Vishal Desai,[1] Srisowmya Sanisetty,[2] Benjamin Steber,[2] Eva Sapi,[2] Bouzid Aliane,[1] Saion Sinha,[3] and Prabir Patra[4,5]

[1] *Department of Electrical and Computer Engineering, University of New Haven, 300 Boston Post Road, West Haven, CT 06516, USA*
[2] *Department of Biology and Environmental Science, University of New Haven, 300 Boston Post Road, West Haven, CT 06516, USA*
[3] *Department of Physics, University of New Haven, 300 Boston Post Road, West Haven, CT 06516, USA*
[4] *Department of Biomedical Engineering, University of Bridgeport, 126 Park Avenue, Bridgeport, CT 06604, USA*
[5] *Department of Mechanical Engineering, University of Bridgeport, 126 Park Avenue, Bridgeport, CT 06604, USA*

Correspondence should be addressed to Saion Sinha, ssinha@newhaven.edu

Received 11 May 2011; Revised 16 July 2011; Accepted 11 August 2011

Academic Editor: Andrei Kolmakov

Nanobiosensors are devices which incorporate nanomaterials to detect miniscule quantities of biological and chemical agents. The authors have already developed a novel bionanosensor (BNS) for quick, efficient, and precise detection of bacterial pathogens using the principles of CNT-DNA interaction and DNA hybridization. The detection ability of the (BNS) was observed to be independent of the device resistance. Two new methods (low-pass filter (LPF) and curve fitting (CF)) were developed for better analysis of the BNS. These methods successfully model the BNS. Evidence is provided to elucidate the success of the model, which can explain the DNA hybridization on the sensor surface. These models successfully demonstrated the detection of DNA hybridization versus nonhybridization. Thus, the models can not only help in better and efficient design and operation of the BNS, but can also be used to analyze other similar nanoscale devices.

1. Introduction

Since the advent of nanotechnology, scientists and engineers have looked forward to the challenges of designing and fabrication of efficient and reliable methods to detect very minute quantities of biological and chemical agents. A nanobiosensor is defined as a device which incorporates nanomaterials for detecting microscopic quantities of biological/chemical agents by measuring changes in the properties of the device [1]. The change is observed primarily in the physical properties of the sensor which is subsequently detected. The two primary methods of response detection for measuring the change of these properties are optical/spectroscopic [2, 3] and electrical [4]. Different types of nanomaterials (e.g., carbon nanotubes, silicon nanowires, TiO_2 nanoparticles, etc.) have been used by researchers [5] to fabricate the sensors. Among the electrical detection methods, some of these techniques measure the electrochemical potential [6], while some others measure the FET transistor characteristics [7]. An economical carbon nanotube- (CNT-) based bionanosensor (BNS) was developed [8] that can precisely and reliably detect biological pathogens. This resistance-based sensor works on the principle of being able to detect DNA hybridization of the pathogen DNAs. The sensor detects the change of the electrical properties of the CNT caused by the wrapping and unwrapping of the single-stranded DNA molecules on CNTs before and after hybridization. The specificity of the BNS has also been demonstrated, by observing that the electrical properties remain unchanged, for a sensor that does not hybridize (referred as nonhybridized sensor). It has also been observed that the specificity and sensitivity of the BNS do not depend on its initial (referred in this paper as bare) resistance. The fabricated BNS had a wide range of bare resistances (50 Ω to 12 KΩ), which did not have any effect on its performance. This paper presents an electrical modeling technique that was developed for understanding the operation of the BNS across such a wide resistance range, including the detection of DNA hybridization [9].

2. Materials and Methods

The BNS (also sometimes referred as the "sensor") were fabricated with multiwalled carbon nanotubes (MWCNT) mats and had a range of resistances. The resistance is dependent on the number of carbon nanotubes. However, the number of carbon nanotubes on each sensor is unknown, as exhibited in SEM micrograph (Figure 1(b)). Moreover, the resistance is affected by the orientation of carbon nanotubes. Consequently, there is an element of randomness built-in to the sensors. The fabrication technique developed was similar for all the BNS's and is independent of the device base resistance. Since the results did not depend on the initial base resistance, it was not required to incorporate precise resistance in the fabrication process. A modified form of solution-casting method was adopted to fabricate the sensor surface. The base adhesive substrate was prepared by mixing 50 mg of tapioca starch to 1000 μL of distilled water and then microwaving (1000 Watt) the solution in two steps. It was initially microwaved for 20 seconds, and then, the process was repeated for another 10 seconds to completely dissolve the tapioca starch and make it into a solution. The tapioca starch solution was then deposited on to the printed circuit board (PCB) sensor area, along with the MWCNT (Catalytic Solutions 99.9%) solution. The solutions were then cured for 30 minutes. On curing, the surface was primed with a thin layer of a single-stranded DNA primer (Borrelia Burgdorferi or Salmonella Enterica), in a buffer solution. Silver paint (Electron Microscopy Sciences, EpoTek) was used for connecting the sensor to the copper terminals of the Printed Circuit Board (PCB). Figure 1(a) is the photograph of the BNS while Figure 1(b) is the scanning electron micrograph of the sensor showing the multiwall carbon nanotubes (MWCNT) networks.

These BNS were driven by the frequency generator (Phillips-PM 5138) in the range of 10 Hz to 10 MHz with input voltage 1 Volt peak-to-peak and the corresponding output was measured on the oscilloscope (Phillips-PM 3377). The voltage gain was measured as a function of frequency by a three-step process. All the measurements were calibrated with reference to the substrate, contacts, and curing conditions. Initially, the gain-frequency response was measured for the bare sensors. Then, the same measurement was made with the sensor primed with the single stranded DNA primer. This is referenced in this paper as the base data. The gain was again measured once the complimentary DNA strand was added. This is the detection stage of the BNS and is referenced in this paper as hybridization stage.

In Figure 2, the gain-frequency characteristics for BNS with a range of different DC resistances are presented for some representative BNS in one graph.

Figure 2 shows that for all the sensors the gain attenuates as the frequency increases. Sensors with lower resistance have higher gain compared to high resistance sensors. For high-resistance sensors (above 2 KΩ), there is a rolloff in gain followed by an extremely small change in gain with respect to frequency.

This characteristic graph also leads us to classify the BNS into two categories based on their resistance. The low-resistance sensors have been classified as devices having resistances of 510 Ω or lower. The high-resistance sensors are devices having resistance value of 800 Ω or higher.

Modeling is a simplified representation of the sensor. It helps to understand the factors responsible for sensor functionality. It allows the prediction of the sensor response, if a certain parameter is changed, and also aids in the improvement of the overall performance. In order to model a sensor, the electronic circuit simulation technique has been used. Circuit simulation is reasonably inexpensive, easily available and not difficult to use, and it also provides fairly accurate and very fast simulation compared to nonelectrical simulation methods. Multidisciplinary processes are complex as it involves transformation from one domain to another (e.g., bond graph simulation, which is a graphical representation of a dynamical system). Thus, it is always beneficial to have the systems simulated under one domain (i.e., circuit simulation).

The sensors have been molded based on two different resistance ranges (low and high resistances) by two different methods, both of which have yielded very similar results. In the first method, the sensor based on a low-pass filter (LPF) using MULTISIM (LPF model) was modeled, while in the second method, the data was mathematically fitted, and then, equations were solved for the circuit parameters using MATLAB (curve fitting model-CF model).

2.1. Modeling the Sensor Based on LPF. As observed, the characteristic curves for all the sensors relate to the characteristics of a LPF [10, 11]. Hence, using the standard formula of a cutoff frequency in a LPF, the sensors were molded

$$f = \frac{1}{2\pi RC}. \tag{1}$$

Here, f = Cutoff frequency in Hertz, R = Resistance in Ω, C = Capacitance in Farads.

From the observed characteristics, curve frequency "f" was determined and for a known value of resistance "R" for sensors, Capacitance "C" was designed. Then, subsequently the sensors were modeled as RC circuits using MULTISIM. The modeled RC circuits were simulated with frequencies ranging from 10 Hz to 10 MHz. The gain-frequency responses for these models were very similar to the patterns that were observed from the experimental data. This can be observed in Figure 3(a), where a model for the 219 Ω sensor has been simulated and then overlaid with the experimental data. Figure 3(b) depicts a similar match for the modeled and the experimental data for high-resistance (11.52 KΩ) sensors.

The RC circuit model of the 219 Ω sensor is demonstrated in Figure 4. As can be observed from the Figure 4, the modeled circuit has capacitance of 68 pF.

Modeling other sensor resistances with the LPF model has also shown a similar response with the experimented data.

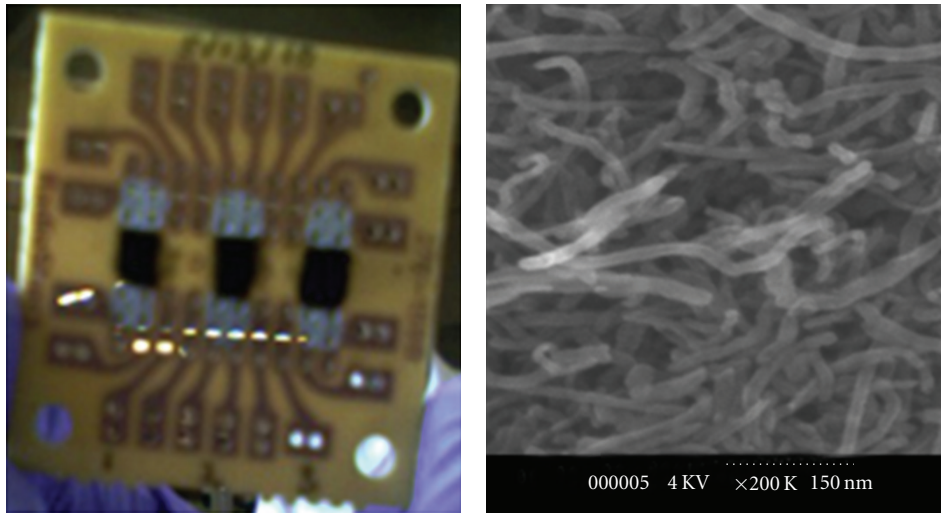

(a) (b)

Figure 1: (a) Photographic image of the BNS depicting 3 sensors which are the black spots in the image. (b) SEM-micrograph of the BNS. This micrograph is of the black regions of (a).

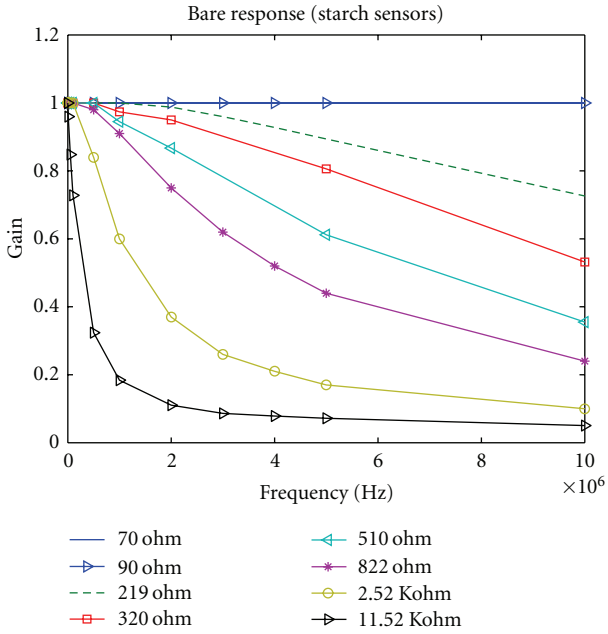

Figure 2: Gain-frequency response for sensors having resistance from 70 Ω to 11.52 KΩ.

2.2. Sensing and Detection with the Sensor. After successfully developing the modeling technique, the sensors were examined for their detection capacity. They were examined using deoxyribonucleic acid (DNA) primers to determine if the model can assist in the determination of DNA hybridization. DNA is a double-stranded biological molecule that has instruction about genes for the biological development of all cellular forms of life [12, 13]. Hybridization is the process where one strand of the DNA (F-DNA) bonds together with the other complementary strands (R-DNA) to form a double helical DNA structure. This bonding combination is very specific and does not occur even if one DNA strand is misaligned by a single base pair. The converse of this hybridization is known as nonhybridization, where the two single-strand DNAs do not combine to form a double helical structure.

Single stranded DNA is known to comfortably wrap around CNT (carbon nanotube) [14]. The process of bonding is energetically favored, through Van der-Waals forces. However, when this F-DNA finds its complementary strand (R-DNA), then the bonding between the DNA strands are significantly stronger (hydrogen bond) which causes the single stranded DNA to unwrap from the CNT and hybridize itself with its complementary primer. This causes a change in electrical properties of the CNT and subsequently the detection efficacy of the BNS. In the DNA nonhybridization process, the F-DNA does not make bonds with its non-complementary (R-DNA) primer and single-stranded DNA continues to wrap around CNT. The electronic property of DNA [15, 16] can lead to some higher order interference, which is not significant in the scale of the BNS.

2.3. Experiments on Sensor with DNAs. The final single strand of DNA (R-DNA) as well as the F-DNA (which was added in the priming process) needs to be delivered in an ionic medium, known as buffer, to keep the DNA intact. For every sensor, the base data was gathered with the sensor being primed by the buffer but without any DNA strands. This is shown in Figure 5 as the "buffer" data.

In Figure 5(a), the gain-frequency plot for a typical low resistance sensor (70 Ω) in the hybridization detection process is presented. Here, it can be observed that the gain-frequency plot shifts downwards (lowering the gain), as the sensor is primed with the F-DNA. It also shifts further downwards on the addition of R-DNA detecting the DNA-hybridization. Hence, it can be inferred that for a low

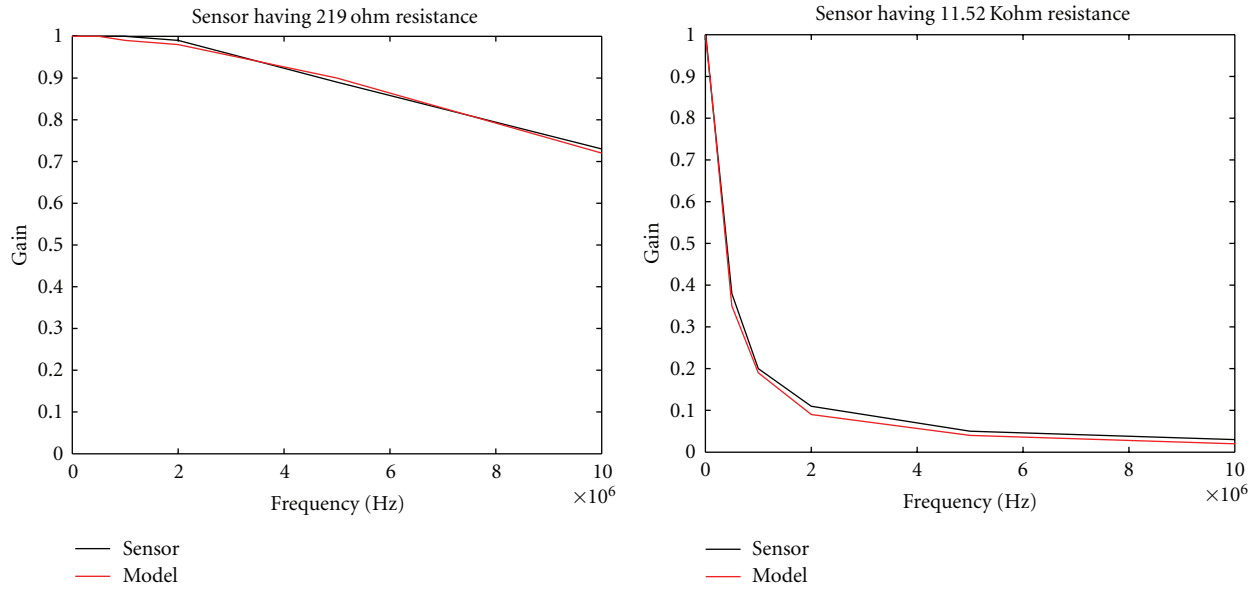

Figure 3: (a) Comparison of the gain-frequency response of a sensor modeled low resistance (219 Ω resistance) with the actual experimental data. (b) Comparison of the gain-frequency response of a sensor modeled high resistance (11.52 KΩ resistances) with the actual experimental data. The "sensor" implies the experimental data, and the "model" implies modeled/simulated data using MULTISIM.

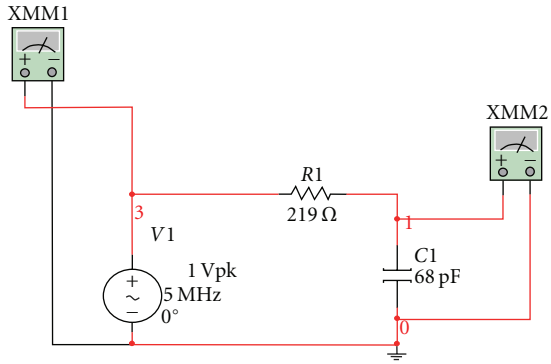

Figure 4: MULTISIM model of sensor having resistance 219 Ω.

resistance sensor the gain decreases with the increase in frequency signaling the detection of DNA-hybridization.

In Figure 5(b), the similar gain-frequency plot for a high resistance sensor (2.52 KΩ) is presented. Contrary to the low resistance sensor, it can be inferred that the gain increases with increase in frequency as sensor detects hybridization.

Similarly, the plots showing DNA nonhybridization is presented in Figure 6. The gain-frequency curves of buffer and R-DNA (nonhybridizing DNA) almost overlap irrespective of their resistances. This behavior shows that the sensors can distinguish between hybridized and nonhybridized DNA.

Note. The hybridizing DNA pair used in the experiment was obtained with Borrelia Burgdorferi (Borrelia-Forward and Borrelia-Reverse (BR)) and the nonhybridizing DNA pair was obtained with Borrelia-Forward (BF) and Salmonella-Reverse (SR).

3. Observation and Results

Based on the gain-frequency characteristics, the sensors were classified as the following:

Group-(1) low resistance sensors: ranging from 10 Ω to 510 Ω.

Group-(2) high resistance sensors: ranging from 800 Ω to 12 KΩ.

Each of these groups was analyzed and modeled by LPF. According to LPF, the capacitance of the equivalent model of the circuit was calculated using a cutoff frequency. As representative example of Group-1, a sensor with 70 Ω bare resistance was chosen. With this cutoff frequency, it was observed that the designed capacitance of the sensor exhibited almost a fivefold increase from 239.3 pF to 1034 pF. This increase is from the base characteristics to the hybridized characteristics of that sensor. Since the Group-2 sensors had a different gain versus frequency characteristics, a 2.52 KΩ bare resistance sensor was chosen as a representative example. In this case the cutoff frequency was iteratively determined from the average of the start and the plateau of the gain behavior. It was also observed that in this case the designed capacitance of the sensor circuit decreases marginally from 18.3 pF to 14.19 pF. To demonstrate the sensing ability of the sensors, nonhybridization DNA data was presented demonstrating that the capacitances of the sensor circuits remained same after adding the R-DNA (nonhybridized).

To authenticate the LPF model, the groups of resistances was alternatively modeled, by a more rigorous and quantitative, curve-fitting model (CF). According to this model, the gain-frequency data was fitted by a second degree polynomial

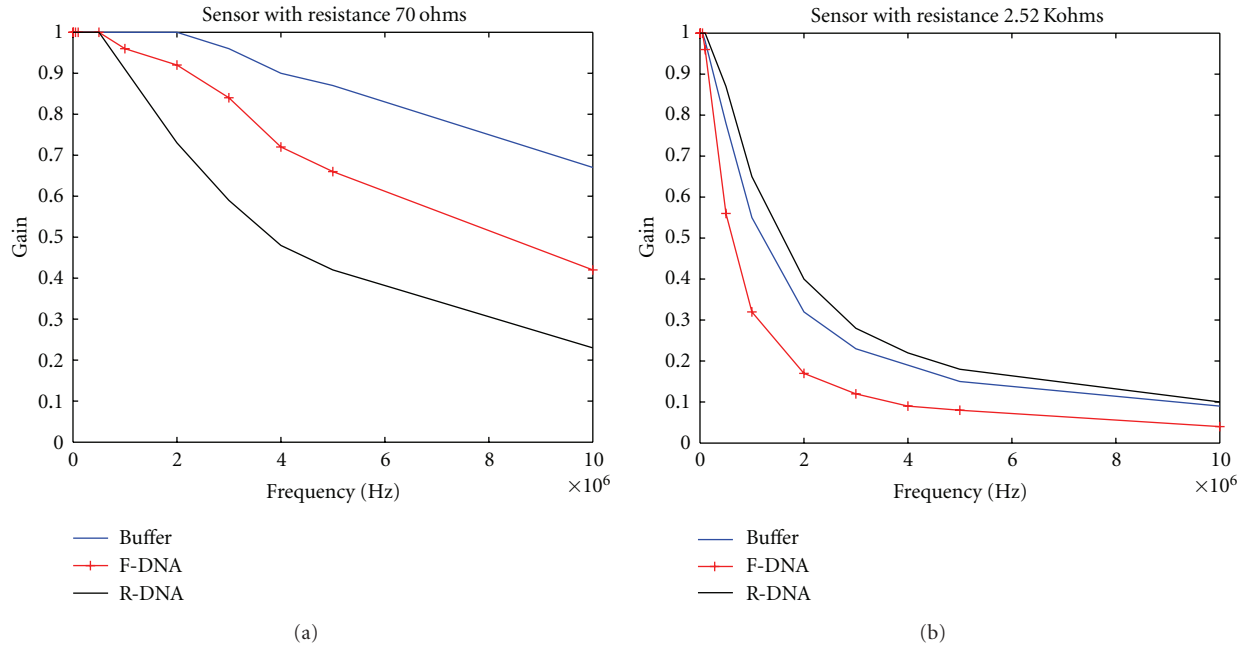

FIGURE 5: (a) The gain versus frequency plot for a low-resistance sensor detecting the DNA hybridization process. It can be observed that the gain of the hybridized sensor is lower than the original (buffer or base). (b) The gain versus frequency plot for a high-resistance sensor in the sensor detecting the DNA hybridization process. It can be observed that the gain of the hybridized sensor is higher than the original (buffer or base).

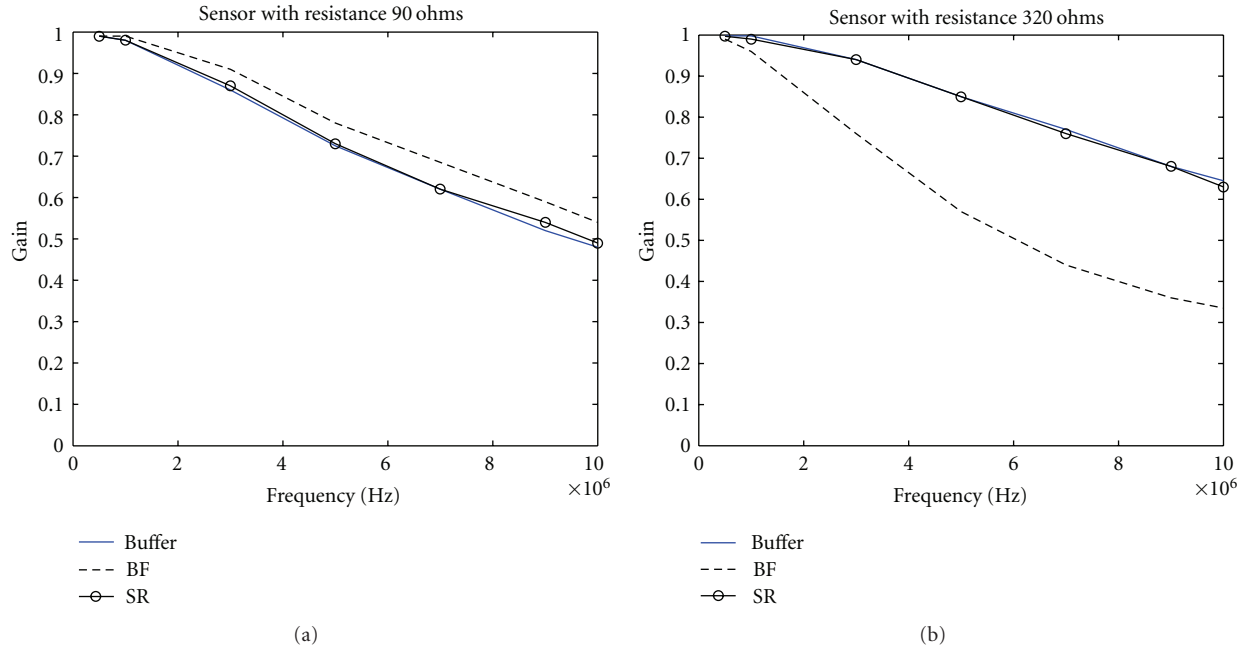

FIGURE 6: (a and b) The gain versus frequency plot for the sensor detecting the DNA nonhybridization process. It can be observed that the gain of the nonhybridized sensor is similar to the original (buffer or base). Each graph represents a sensor with different resistance.

(quadratic) for the Group-1 and Group-2 sensors. This polynomial equation was solved to determine the cutoff frequency which was then subsequently used to design the capacitance equivalent of the sensor circuit. The algorithm for curve fit technique is explained below.

The equation of the gain-frequency relation for the quadratic curve fit is given as follows:

$$y = az^2 + bz + k, \tag{2}$$

where, y is the gain (Known); a, b and k are constants.

Table 1: The capacitance calculated from the circuit models (LPF and CF) for a low resistance sensor.

	Capacitor (designed)	Capacitor (calculated)
BASE	239.3 pF	229.75 pF
Hybridized DNA	1034 pF	1038 pF

Table 2: The capacitance calculated from the circuit models (LPF and CF) for high resistance sensors.

	Capacitance (designed)	Capacitance (calculated)
BASE	18.3 pF	18.31 pF
Hybridized DNA	14.19 pF	16.21 pF

Table 3: (a and b) The capacitance calculated from the circuit models (LPF and CF) for nonhybridizing DNA sensors.

(a)

90 Ω resistance	Capacitance (designed)	Capacitance (calculated)
BASE	313 pF	322 pF
Nonhybridized DNA	313 pF	316 pF

(b)

320 Ω resistance	Capacitance (designed)	Capacitance (calculated)
BASE	58 pF	58 pF
Nonhybridized DNA	58 pF	58 pF

And

$$z = \frac{x - m}{n}, \tag{3}$$

where frequency (x) is scaled through (3) using MATLAB; (m) and (n) are constant scaling factors. Equation (2) is reduced to

$$az^2 + bz + k - y = 0. \tag{4}$$

Since (k) and (y) are constants, using $k - y = c$ and simplifying (4) yields

$$az^2 + bz + c = 0. \tag{5}$$

The roots of this equation are

$$z = \frac{-b \pm \sqrt{b^2 - 4ac}}{2a}. \tag{6}$$

Substitution of (3) in (6) will produce

$$x = \left[\frac{-b \pm \sqrt{b^2 - 4ac}}{2a}\right] * n + m. \tag{7}$$

Equation (7) has two roots. Since (x) is a frequency, it can also be matched to the LPF model

$$x = \frac{1}{2\pi RC}. \tag{8}$$

Substituting (8) in (7), the value of capacitance (C) can be evaluated for a given resistance value. Following is the curve fit solver for low- and high-resistance sensors.

Figures 7(a) and 7(b) show how the curve-fitting model compares with the experimental data for the base and hybridized sensor, respectively. The quadratic equations are illustrated under the curves. Table 1 shows the value of the capacitances calculated (LPF) and the designed (CF) for the two models. It can be observed that there is a close match between the values.

Figures 8(a) and 8(b) are the graphs showing the curve fitting model with the experimental data for the base and hybridized for a high-resistance sensor, respectively. The second degree polynomial was the closest fit for the relevant cutoff frequency regions of the gain-frequency graph. The equations are illustrated under the respective curves and the calculated (LPF) and designed (CF) values of capacitances are shown in Table 2. These values are quite similar, thus, demonstrating a close match of the models.

Similar comparison processes for calculating the capacitances between the LPF and CF models were applied, for the sensors where nonhybridization experiments were performed. Table 3 shows the designed and calculated capacitance for nonhybridizing sensors. There was a close match between the designed and calculated capacitance values authenticating the LPF model.

4. Discussion

On combining the experiments with the modeling parameters, the following were observed.

The low resistance sensors on being hybridized, that is, after receiving second primer (R-DNA), show an increment in the value of capacitance, whereas for very high resistance sensors, there is a decrement in the value of capacitance. Figures 9(a) and 9(b) histogram plots indicating the changes in capacitance for very low and high resistance sensors. The capacitance remains constant when there is *no* DNA hybridization (nonhybridization) occurring on the sensor. This behavior is illustrated in Figures 10(a) and 10(b), respectively. Thus, the BNS detects DNA hybridization by a change in the capacitances, and this process is independent of the bare resistances of sensors.

The reason for the different trends in the capacitor change is critical in understanding the operation and performance of a BNS. The change in the capacitance can be understood using the RC circuit model. Figure 11 is the circuit model which is applicable to both very low- and high-resistance sensors.

After adding buffer; the capacitance for both; very low- and very high-resistance sensor increases [17]. The sensor is cured after it receives buffer and that causes buffer to spread throughout the sensor. Once the AC voltage is applied, the capacitance caused by buffer will experience the same voltage as of the capacitance caused by the bare sensor. This gives the base capacitance of the sensor. In the case of the low-resistance sensors, it was observed that the gain depends

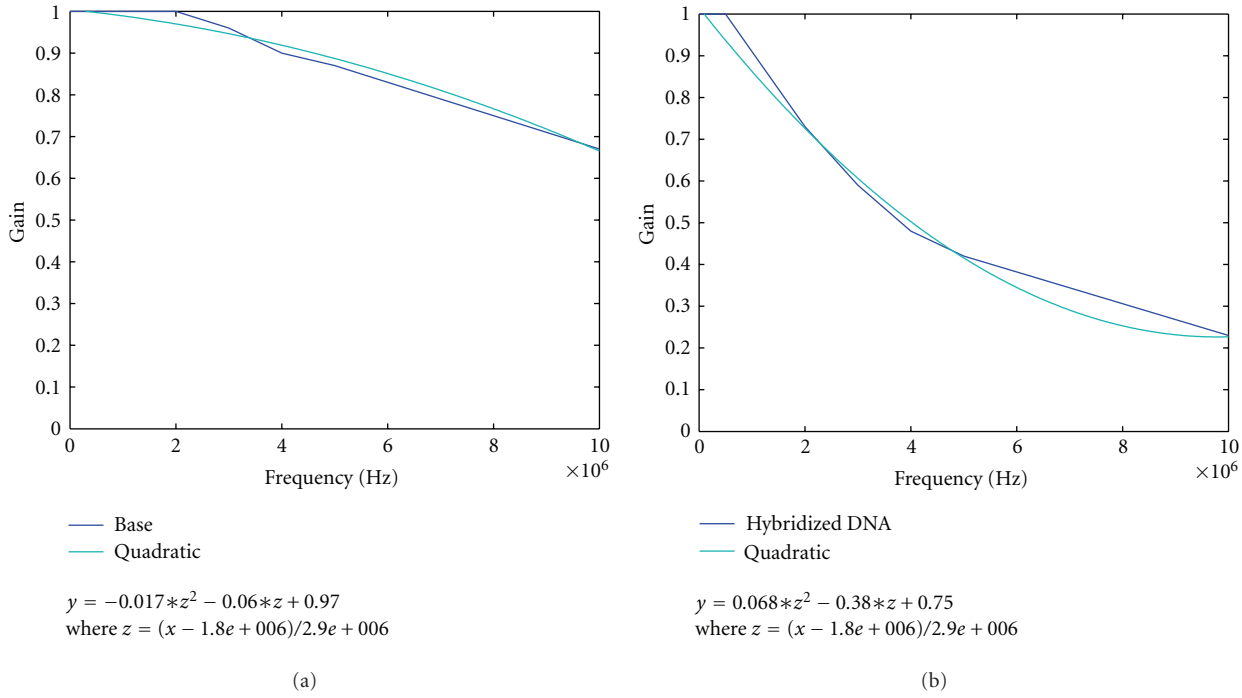

FIGURE 7: (a) and (b) represent the curve fitting technique applied on the 70 Ω Base and Hybridized sensor, respectively. Equations underneath respective figures represent the gain-frequency relationship. Using the above equations, the capacitance for the sensor with known resistance was calculated and it resulted in a value comparable to the designed capacitance. Table 1 represents the designed and calculated capacitance (from above equations).

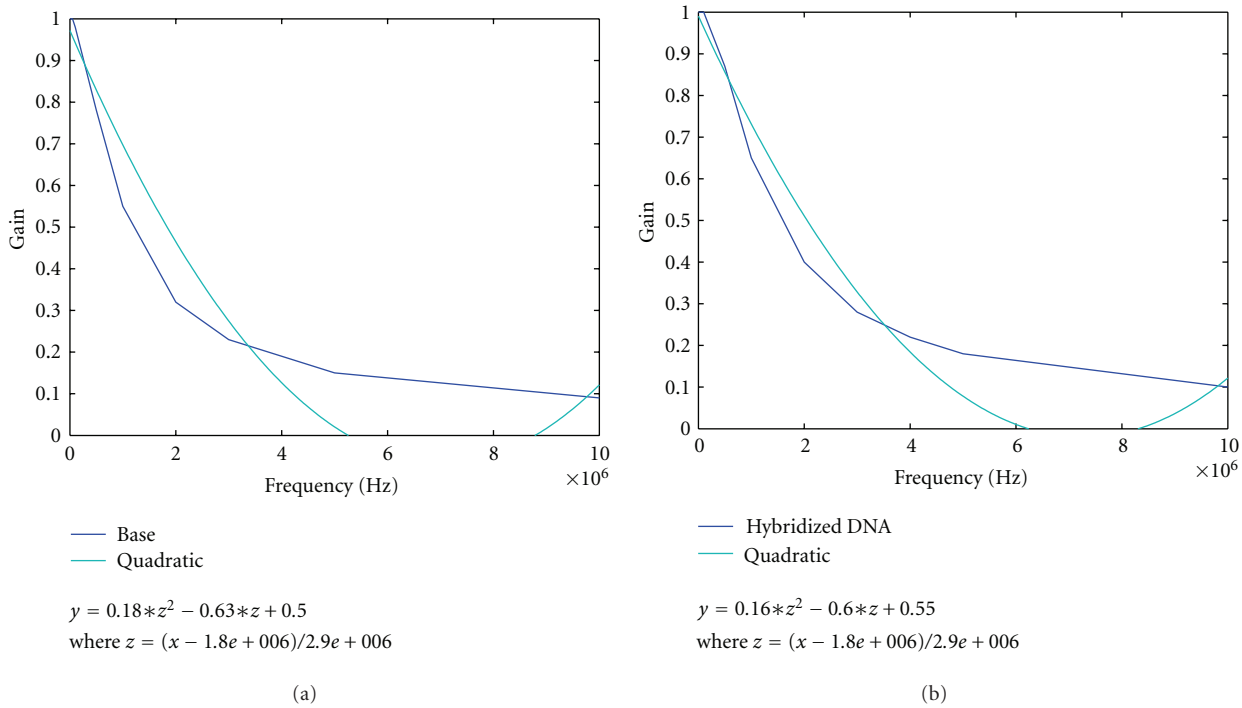

FIGURE 8: (a) and (b) represent the curve fitting technique applied on the 2.52 KΩ bare and hybridized Sensor, respectively. Equations below the respective figures represent the gain-frequency relationship. Using the above equations, the capacitance for the sensor with known resistance (2.52 KΩ) was calculated, and it was closely comparable with the designed value of capacitance. Table 2 represents the designed and calculated capacitance.

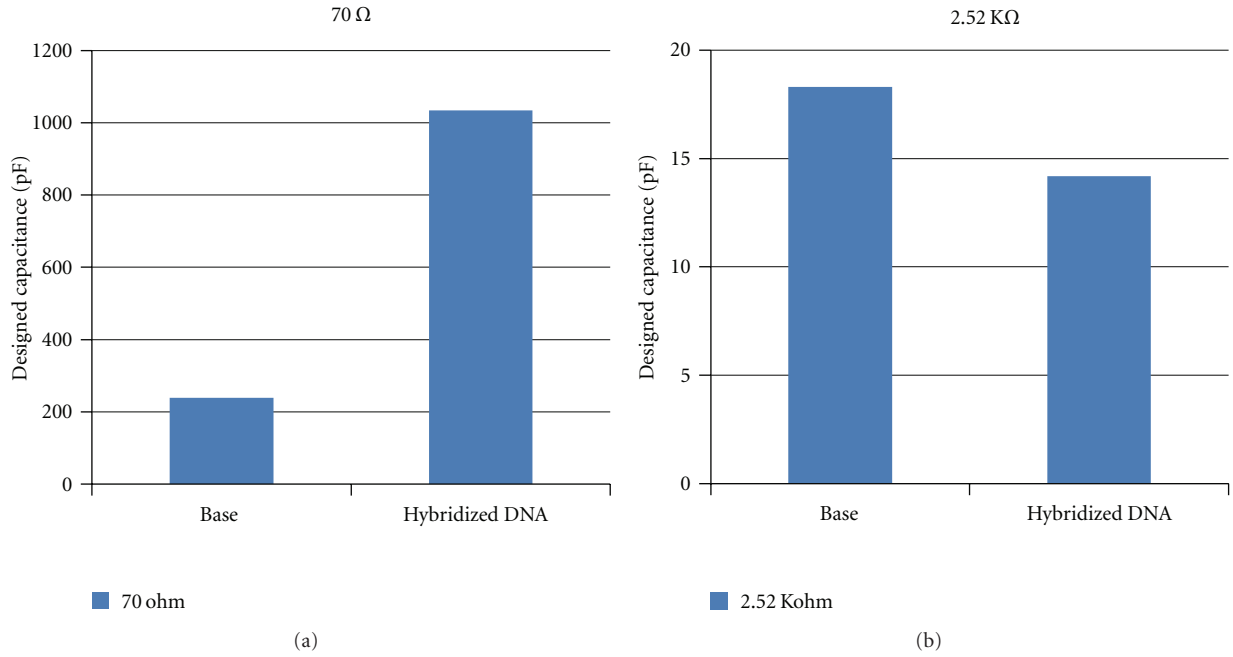

Figure 9: (a) Designed capacitance change from BASE to hybridized DNA for sensor having 70 Ω bare resistance. (b) Designed capacitance change from BASE to hybridized DNA for sensor having 2.52 KΩ bare resistance.

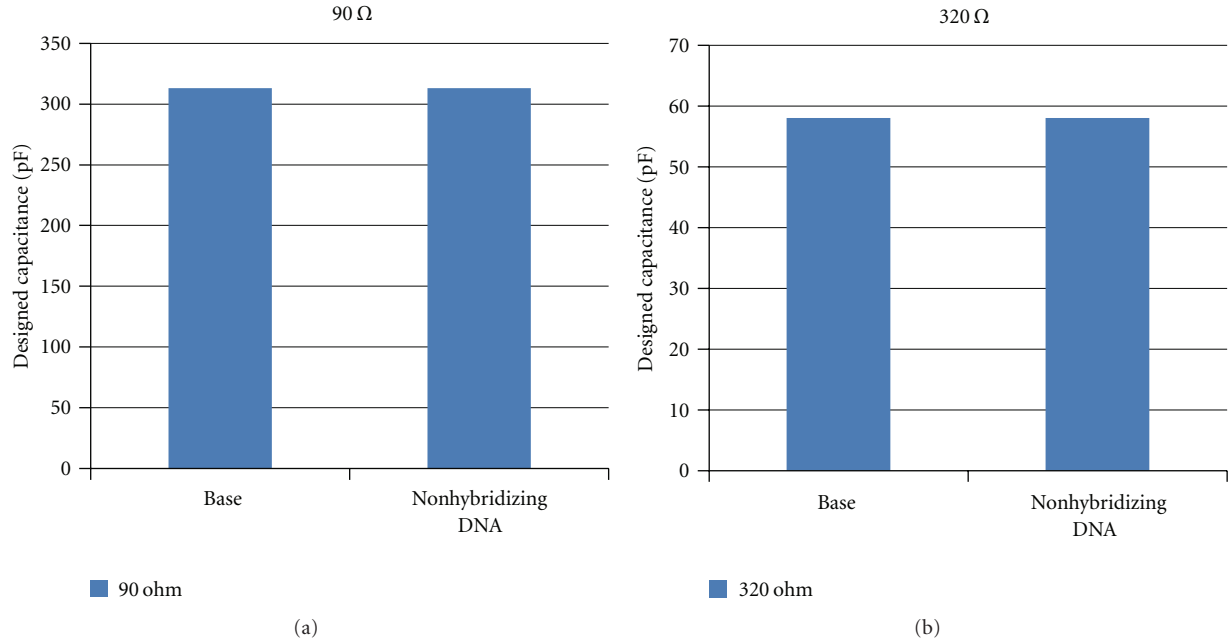

Figure 10: (a) Designed capacitance remains the same from BASE to hybridized DNA for sensor having 90 Ω bare resistance. (b) Designed capacitance remains the same from BASE to hybridized DNA for sensor having 320 Ω bare resistance.

on the frequency, and so, the impedance of the sensor is predominantly capacitive.

From the models (LPF and CF) discussed earlier, it was observed that on hybridization, the capacitance of the sensor increases by almost a fivefold for the low-resistance sensors. Hybridization occurs when the complementary primer (R-DNA) is added to the sensor. At this stage the F-DNA, which was already on the surface of the sensor, wrapped around CNTs leaves the host (CNT) and starts bonding with the F-DNA. This creates additional parallel channels of capacitance. Some of these new capacitance channels are quite large, since it is created from the void left over by the F-primer. The extra channel capacitance, is connected in parallel to the earlier capacitances of the base sensor,

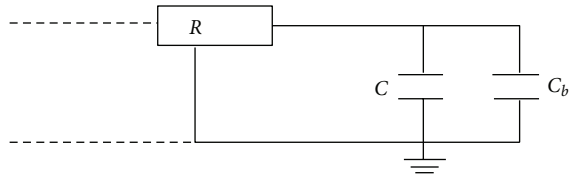

Figure 11: RC model for sensor with C_b (buffer capacitance) in parallel.

and hence increases the overall capacitance of the hybridized sensor.

The gain for the high-resistance sensors remains constant over the major frequency domain (after the initial drop), where the measurement was performed. This implies that the impedances of these sensors are not frequency dependent and, therefore, are primarily resistive. Hence in the hybridization stage the unwrapping of the DNA does not cause any significant increase of the capacitance. This is possible only when the additional small capacitance caused by the hybridization is connected in series to the original capacitance of the base sensor. This leads to a small decrease in capacitance of the hybridized sensor which matches with the experimental observation.

However, for the nonhybridization process, the capacitance of R-DNA was similar to that of the buffer. The F-DNA on the MWCNTs will not make any bonds with R-DNA, and as a result, the R-DNA will again wrap around the MWCNT. This will neutralize the capacitance caused by the F-DNA, and hence, the final capacitance is same as the buffer capacitance.

5. Conclusion

Successful frequency dependent models showing the operation of the BNS were developed. The models were able to analyze data for both low- and high-resistance sensors and hence were independent of sensor resistances. The results from both the electrical circuit models (LPF and CF) were consistent with each another. The CF model is more quantitative and can provide information on the concentration of the hybridized and nonhybridized DNA in a particular sample. Both of these models hypothesized the BNS to be working like an RC circuit with the capacitance playing a major role in the results. Even though the characteristic curves of the low- and high-resistance sensors are very different from each other the sensor performance, it is independent of their resistances. The modeling not only aids in understanding the working principle of the sensor but also enables its efficient design leading to the optimal operation frequency range. These models will be very useful in studying other types of sensors leading to their optimal performance.

Acknowledgment

The authors wish to acknowledge University of New Haven for providing support and funding for this project.

References

[1] A. S. Bassi and G. K. Knopf, Eds., *Smart Biosensor Technology*, CRC Press, New York, NY, USA, 2007.

[2] H. Kurzbauer, "Banishing the wolf," *Strad*, vol. 114, no. 1357, pp. 486–487, 2003.

[3] J. L. West and N. J. Halas, "Engineered nanomaterials for biophotonics applications: improving sensing, imaging, and therapeutics," *Annual Review of Biomedical Engineering*, vol. 5, pp. 285–292, 2003.

[4] P. Alivisatos, "The use of nanocrystals in biological detection," *Nature Biotechnology*, vol. 22, no. 1, pp. 47–52, 2004.

[5] A. M. Morales and C. M. Lieber, "A laser ablation method for the synthesis of crystalline semiconductor nanowires," *Science*, vol. 279, no. 5348, pp. 208–211, 1998.

[6] H. Cai, X. Cao, Y. Jiang, P. He, and Y. Fang, "Carbon nanotube-enhanced electrochemical DNA biosensor for DNA hybridization detection," *Analytical and Bioanalytical Chemistry*, vol. 375, no. 2, pp. 287–293, 2003.

[7] T.-C. Lim, Ed., *Nanosensors: Theory and Applications in Industry, Healthcare and Defense*, CRC Press, New York, NY, USA, 2010.

[8] S. Sinha and E. Sapi, "Bionanosensor detection device," U.S. Patent/WO2010/039941.

[9] M. Meyyappan, Ed., *Carbon Nanotubes Science and Applications*, CRC Press, New York, NY, USA, 2004.

[10] J. C. Whitaker, *The Resource Handbook of Electronics*, CRC Press, New York, NY, USA, 2001.

[11] S. Kumar, *Digital Signal Processing: A Computer Based Approach*, McGraw-Hill, New York, NY, USA, 2006.

[12] Y. Xu, X. Mi, and N. R. Aluru, "Detection of defective DNA in carbon nanotubes by combined molecular dynamics/tight-binding technique," *Applied Physics Letters*, vol. 95, no. 11, Article ID 113116, 3 pages, 2009.

[13] A. Datta and E. R. Dougherty, *Introduction to Genomic Signal Processing with Control*, CRC Press, New York, NY, USA, 2007.

[14] M. Zheng, A. Jagota, M. S. Strano et al., "Structure-based carbon nanotube sorting by sequence-dependent DNA assembly," *Science*, vol. 302, no. 5650, pp. 1545–1548, 2003.

[15] G. Dekker and M. A. Ratner, "Electronic properties of DNA," *Physics World*, vol. 14, no. 8, pp. 29–33, 2001.

[16] N. P. Armitage, M. Briman, and G. Grüner, "Charge transfer and charge transport on the double helix," *Physica Status Solidi (B) Basic Research*, vol. 241, no. 1, pp. 69–75, 2004.

[17] J. Hong, D. S. Yoon, M. I. Park et al., "A dielectric biosensor using the capacitance change with AC frequency integrated on glass substrates," *Japanese Journal of Applied Physics*, vol. 43, no. 8, pp. 5639–5645, 2004.